

Repressed miR-34a Expression Dictates the Cell Fate to Corneal Endothelium Failure

Junji Hamuro,¹ Kazuko Asada,¹ Morio Ueno,¹ Tomoko Yamashita,² Atsushi Mukai,¹ Tomoko Fujita,¹ Eiko Ito,¹ Nao Hiramoto,¹ Munetoyo Toda,² Chie Sotozono,¹ and Shigeru Kinoshita²

¹Department of Ophthalmology, Kyoto Prefectural University of Medicine, Kyoto, Japan

²Department of Frontier Medical Science and Technology for Ophthalmology, Kyoto Prefectural University of Medicine, Kyoto, Japan

Correspondence: Junji Hamuro, Department of Ophthalmology, Kyoto Prefectural University of Medicine, 465 Kajii-cho, Hirokoji-agaru, Kawaramachi-dori, Kamigyo-ku, Kyoto 602-0841, Japan; jshimo@koto.kpu-m.ac.jp.

Received: December 15, 2021

Accepted: April 13, 2022

Published: April 27, 2022

Citation: Hamuro J, Asada K, Ueno M, et al. Repressed miR-34a expression dictates the cell fate to corneal endothelium failure. *Invest Ophthalmol Vis Sci.* 2022;63(4):22. <https://doi.org/10.1167/iovs.63.4.22>

PURPOSE. To reveal the mechanism triggering the functional disparity between degenerated and non-degenerated corneal endothelium cells in the water efflux from corneal stroma to the anterior chamber.

METHODS. The varied levels of the microRNA (miR)-34, miR-378, and miR-146 family in human corneal endothelium and cultured cells thereof were investigated using 3D-Gene Human miRNA Oligo Chips. Concomitantly, CD44, p53, c-Myc, matrix metalloproteinase (MMP)-2 expression, and Ras homolog gene family member A (Rho A) activity was correlated to the expression intensities of these microRNAs, partly complemented with their altered expression levels with the transfection of the corresponding mimics and inhibitors. The levels of miRs were further associated with intracellular pH (pHi) and mitochondrial energy homeostasis.

RESULTS. P53-inducible miR-34a/b repressed CD44 expression, and CD44 was repressed with the elevated c-Myc. The repressed miR-34a activated the CD44 downstream factors Rho A and MMP-2. MiR-34a mimics downregulated pHi, inducing the skewing of mitochondrial respiration to oxidative phosphorylation. The oxidative stress (H₂O₂) induced on human corneal endothelial cells, which repressed miR-34a/b expression, may account for the impaired signaling cascade to mitochondrial metabolic homeostasis necessary for an efficient water efflux from the corneal stroma.

CONCLUSIONS. The upregulated expression of CD44, through repressed miR-34a/b by reactive oxygen species and elevated c-Myc by oxidative stress, may impair mitochondrial metabolic homeostasis, leading to human corneal endothelial failure.

Keywords: CD44 and miRNA, mitochondria metabolic homeostasis, human corneal endothelium failure, intracellular pH, oxidative stress

A single layer of human corneal endothelial cells (HCECs) in the human corneal endothelium (HCE) forms a barrier between the corneal stroma and aqueous chamber (AC).^{1,2} HCECs are metabolically active and facilitate a pumping action with an active efflux of ions from the corneal stroma into the AC,³ thereby preventing stromal overhydration to maintain corneal transparency. HCEC attrition beyond approximately 500 cells/mm² results in endothelial decompensation.⁴

Allogeneic corneal transplantation, or keratoplasty, is currently the standard clinical modality for patients with corneal endothelial degeneration.⁵⁻⁷ Several new modalities have been recently reported, including cell therapy by cultured HCECs (cHCECs).^{8,9}

The putative population of endothelial progenitors can harbor stem cell-like or dedifferentiated cell characteristics in the peripheral HCE or cHCECs.^{4,10,11} We have proposed a new avenue to achieve efficient in vitro propagation through the dedifferentiation of mature HCECs into progenitor-like

cells, followed by the differentiation of thus induced immature proliferative (progenitor) HCECs into mature differentiated HCECs.^{10,11} Propagated cHCECs are relatively homogeneous compared to directly expanded cHCECs, which tend to be a mixture of subpopulations (SPs) with distinct cell-state transition (CST) phenotypes.¹² We have successfully identified cHCEC SPs with high clinical efficacy (occasionally described as effector cells) versus those with low clinical efficacy.^{9,13} We have also specified the effector cell cHCEC SPs with CD133, CD105, CD90, CD44, CD26, CD24, and human leucocyte antigen (HLA)-DR as negative and CD166, HLA-ABC, and programmed cell death ligand 1 (PD-L1) as positive, as well as the manufacturing approach thereof.^{12,14,15}

Mitochondrial oxidative phosphorylation (OXPHOS) in mature differentiated SPs is more dominant, whereas both glycolysis and OXPHOS are elevated in cHCEC SPs with CST,^{10,11,16} including dedifferentiation, epithelial-mesenchymal transition (EMT), immaturity, and cell

senescence. The preliminary proteome analysis has revealed that functionally critical ion channels and transporters—solute carrier family 4 member 11 (SLC4A11), aquaporin 1 (AQP1), and Na⁺/H⁺ exchanger 1 (NHE1)—are selectively polarized in mature differentiated cHCEC SPs.^{1,17} AQP1 and SLC4A11, together with the ordered expression of zonula occludens-1 (ZO-1), on HCE are critical players engaging in the water efflux from the corneal stroma into the AC.¹⁸ *SLC4A11* is mutated in late-onset Fuchs' corneal dystrophy and in the congenital hereditary endothelial dystrophy (CHED) of corneal endothelium.^{19–23} Individuals with CHED have mutations in *SLC4A11*, which encodes a transmembrane protein in the SLC4 family of bicarbonate transporters.

There are several reports that intracellular pH (pHi) is related to mitochondrial respiratory functions and indirectly to cell differentiation.^{24–32} The maintenance of glycolysis and OXPHOS-processing enzymes is highly dependent on pHi. In this context, our recent study has revealed that pHi regulates not only the HCEC fate, such as differentiation versus CST, dedifferentiation, or EMT, but also mitochondrial metabolic homeostasis; consequently, it is associated with efficient water efflux in cell therapy from the corneal stroma into the AC by the injection of mature differentiated cHCEC SPs.¹⁷

In the present study, we revealed the molecular mechanisms underlying HCE failures—namely, the functional disparity between degenerated and non-degenerated HCECs. We confirmed that p53-inducible microRNA (miR)-34a downregulates CD44 expression in a concerted manner with the elevated c-Myc and that the miR-34a/CD44 axis activates the downstream factors of CD44, including Ras homolog gene family member A (Rho A) and matrix metalloprotease (MMP)-2. In addition, MiR-34a mimics downregulate pHi, inducing the polarization of mitochondrial respiration to OXPHOS.^{25,33} The oxidative stress imposed on the cHCECs depressed miR-34a expression.

MATERIALS AND METHODS

HCEC Donors, Cell Cultures, and Flow Cytometry Analysis

The human tissue used in this study was handled in accordance with the tenets set forth in the Declaration of Helsinki. Human donor corneas were obtained from CorneaGen, Inc. (Seattle, WA, USA), as described in the Supplementary Section (Supplementary Table S1). Unless stated otherwise, the HCECs were cultured according to the published protocols.^{10,12,14,15} The 30 lots of cHCECs used in this study are summarized in Supplementary Table S2. All procedures for flow cytometry analysis were the same as described previously.¹⁴ Phase-contrast microscopy images were captured using the Olympus CKX41 Inverted Microscope (Olympus Corporation, Tokyo, Japan).

Cell Fractionation

Cell fractionation was performed using a nuclear/cytosol fractionation kit (K266-25; BioVision, Milpitas, CA, USA) according to the manufacturer's instructions. In brief, the cells were lysed and the cell suspension was centrifuged at 15,000g for 5 minutes. The resulting supernatant was then collected as the cytosol fraction. The cytosol-depleted pellet was solubilized in nuclear extraction buffer. Follow-

ing centrifugation at 15,000g for 10 minutes, the supernatant was collected as the nuclear fraction. Fraction purity was analyzed by immunoblotting. Histone H3 and β -actin were used as nuclear and cytosol-specific markers, respectively.

Western Blotting of p53, p21, Rho A, and MMP-2

The basic procedures are the same as described previously.^{10,14–16} The primary antibodies were obtained as follows: Na⁺/K⁺-ATPase (#05-369; Merck KGaA, Darmstadt, Germany); β -actin (#4967), heme oxygenase-1 (HO-1; #5061), p53 (#9282), phospho-p53 (Ser15; #9284), phospho-H2A histone family member X (H2AX, Ser139; #9718), sirtuin 1 (SIRT1; #9475), p21 (#2946), and mitochondrial transcription factor A (TFAM; #8076) from Cell Signaling Technology (Danvers, MA, USA); c-Myc (ab32072), DJ-1 (ab18275), Kelch-like ECH-associated protein 1 (Keap1; ab66620), nuclear factor erythroid 2-related factor 2 (Nrf2; ab62352), translocase of outer mitochondrial membrane 20 (TOMM20; ab56783), and voltage-dependent anion channel (VDAC; ab235143) from Abcam (Cambridge, UK); histone H3 (#05-928; MilliporeSigma, Temecula, CA, USA); PGC1- α (NBP1-04676; Novus Biologicals, Littleton, CO, USA); and Rho A (ab54835) and MMP-2 (ab92536) from Abcam. Goat anti-mouse immunoglobulin G (IgG) and goat anti-rabbit IgG (H+L; Southern Biotech, Birmingham, AL, USA) were used as the secondary antibodies. MagicMark XP Western Protein Standard (Thermo Fisher Scientific, Waltham, MA, USA) was used as the molecular weight marker. The protein bands were made visible by a Western BLoT HRP substrate series (TakaraBio, Shiga, Japan).

Enzyme-Linked Immunosorbent Assay and Mitochondrial Respiration Assay

Enzyme-linked immunosorbent assays and mitochondrial respiration assays were performed as described previously.^{10,11,14} The oxygen consumption rate (OCR) and extracellular acidification rate (ECAR) were analyzed according to the manufacturer's protocol using the Seahorse XFe24 Analyzer (Agilent Technologies, Santa Clara, CA, USA).^{11,14}

Quantitative Real-Time Polymerase Chain Reaction and MicroRNA Expression Profiling

Polymerase chain reaction (PCR) was performed under the conditions described previously.^{10–12} The levels of miR-34a, mir-34b, mir-378a, CD44, p53, IL-8, platelet-derived growth factor (PDGF)- $\beta\beta$, vascular endothelial growth factor (VEGF), and Rho A were normalized to that of glyceraldehyde-3-phosphate dehydrogenase (GAPDH), and the results were presented as 2^{− Δ Ct} (relative units of expression). The primers used are listed in Supplementary Table S3 by the assay IDs of the manufacturers.

For miRNA expression profiling, 3D-Gene Human miRNA Oligo Chips (miRBase version 17-21; Toray Industries, Inc., Tokyo, Japan) were used, and the other procedures were the same as those described previously.³³

Transfection of miR Mimics or Inhibitors

The transfection of both miR mimics and miR inhibitors at 30 nM was conducted using the Lipofectamine RNAiMAX reagent (Thermo Fisher Scientific) according to the manu-

facturer's protocol. The mimics and inhibitors targeting miR-34a, miR-34b, miR-378a, and negative control mimics or inhibitors were purchased from Thermo Fisher Scientific. Each vector plasmid was combined with each miRNA transfection by using a DharmaFECT Duo reagent (GE Healthcare Dharmacon, Lafayette, CO, USA) in accordance with the manufacturer's protocol.

Detection of p53 and p21 Proteins Induced by Nutlin-3a

Immature cHCEC SPs at the proliferative stage with CD44^{+/+/+} (71.5%) were stimulated with a mouse double minute 2 homolog (MDM2) inhibitor, Nutlin-3a, for 24 hours, and the induction of p53 and p21 proteins was monitored by western blotting (WB). The direct monitoring of p53 activity in both mature and immature cHCEC SPs had been unsuccessful; therefore, this indirect method was adapted to monitor the induction of p21 protein, which is known to be in parallel with p53 activity.^{34,35} Cells ($5-7 \times 10^5$ /mL) were cultured for 24 hours with the indicated concentrations of Nutlin-3a, and whole cell lysate (40 mg) was prepared. The expression levels of p53-related proteins were detected using WB analysis, and those of miR-34a and miR-34b were detected by quantitative real-time polymerase chain reaction (qRT-PCR). The stimulation level (fold induction) was determined by setting the value without Nutlin-3a as 1.0. Experiments were performed in duplicate, and the results are expressed as mean \pm SD.

Rho A Activation Assay

Cells grown under normal conditions were treated in serum starvation conditions (1% fetal bovine serum [FBS]) for 6 hours, after which the samples were collected and preserved through snap-freezing in liquid nitrogen. After the protein quantity was made equivalent across all samples by measuring the protein concentration using a Bradford reagent through a NanoDrop spectrophotometer (immunoblotting; Thermo Fisher Scientific), Rhotekin-RBD beads and other reagents from the RhoA Pull-Down Activation Assay Biochem Kit (#BK036-S; Cytoskeleton, Inc., Denver, CO, USA) were added to the protein lysates and then centrifuged as described in the product protocol according to the manufacturer's instructions. WB was then performed on the proteins that remained bound to the beads, using a special Rho A primary antibody provided by the manufacturer.

Immunocytochemical Detection of MMP-2

To compare the correlation of the expression of miR-34a and MMP-2, cHCEC SPs with either high or low expression of intracellular miR-34a were fixed for 10 minutes at -30°C with cold methanol and then blocked with 1% FBS in Dulbecco's phosphate-buffered saline (Nacalai Tesque, Kyoto, Japan) for 60 minutes at room temperature. The cells were then stained overnight at 4°C with anti-MMP-2 antibody (1:100), followed by staining for 60 minutes at room temperature with a second antibody, FITC Goat Anti-Mouse IgG (1:1000; Abcam). The cells were then viewed by fluorescence microscopy (BZ-9000 Fluorescence Microscope; Keyence, Osaka, Japan).

Measurement of pHi of cHCECs

The pHi of cHCEC SPs was measured using the cell-permeable probe 3'-O-acetyl-2',7'-bis(carboxyethyl)-5,6-carboxyfluoresceinacetoxymethyl ester (BCECF-AM special packaging; Dojindo Chemical Co., Ltd., Tokyo, Japan) following the manufacturer's instructions.¹⁰ We used the Dojindo Assay Kit (Dojindo Molecular Technologies, Inc., Tokyo, Japan). The procedures for calibrating BCECF fluorescence have been detailed previously.¹⁰

Statistical Analysis

A Student's *t*-test was conducted to determine the statistical significance (*P* value) of the mean values for two-sample comparisons, and Dunnett's multiple-comparison test was conducted to determine the statistical significance for the comparison of multiple sample sets. Values shown in the graphs represent mean \pm SE.

RESULTS

Repression of miR-34a/b and miR-378a in HCE Tissues

First, we assessed the expression levels of miR-34a/b-5p and miR-378-3p and three isoforms of control miR-146 (a-5p, b-3p, and b-5p) in HCE tissues distinct in their tissue endothelial cell density (ECD; 3145, 1463, and 949 cells/mm², respectively) (Fig. 1A). The statistically significant repressed expression levels of miR-34a-5p and miR-34b-5p were confirmed in HCE tissues with reduced ECD, in contrast to the absence of repressed expression of miR-146 isoforms. Considering the hypothetical mimicry between in vitro CST cHCECs and degenerated HCE tissues with lowered ECD and/or guttae, we next compared the miR profiles in cHCEC SPs distinct in the proportion of CD44^{-/dull} cells (E-ratios). The downregulation of miR-34a/b-5p and miR-378-3p was statistically significant in CST cHCECs, whereas the three isoforms of reference miR-146 (a-5p, b-3p, and b-5p) were not downregulated (Fig. 1B). Thus, it is rational to deduce that the downregulation of the former three miRs in freshly degenerated HCE tissues with lowered ECD and/or guttae can be comparably simulated by those in CST cHCECs.

Repressed Expression Levels of miR-34a/b and miR-378a in cHCEC SPs

We have previously reported the distinctly staged proliferation, differentiation, and maturation of dedifferentiated cHCEC SPs during cultures.¹¹ Consequently, the periodic alteration of the expression levels of miR-34a-5p, miR-34b-5p, and miR-378-3p during the culture stages was monitored. The expression levels of the latter two miRs were found to be already elevated at the differentiation stage on day 21, whereas miR-34a-5p was only elevated at the maturation stage on day 42 (Fig. 2A). The altered expression levels of these miRs were also recognized among cHCEC SPs distinct in terms of CD44 expression levels (93.4%, 50%, and 21.6%, respectively) (Fig. 2B). With the aim to elucidate the dependency of expression profiles of miRs on the SP composites distinct in their differentiation/maturation stages, RNA extracted from fluorescence-activated cell sorter (FACS)-defined cHCEC SPs was used for the 3D-Gen

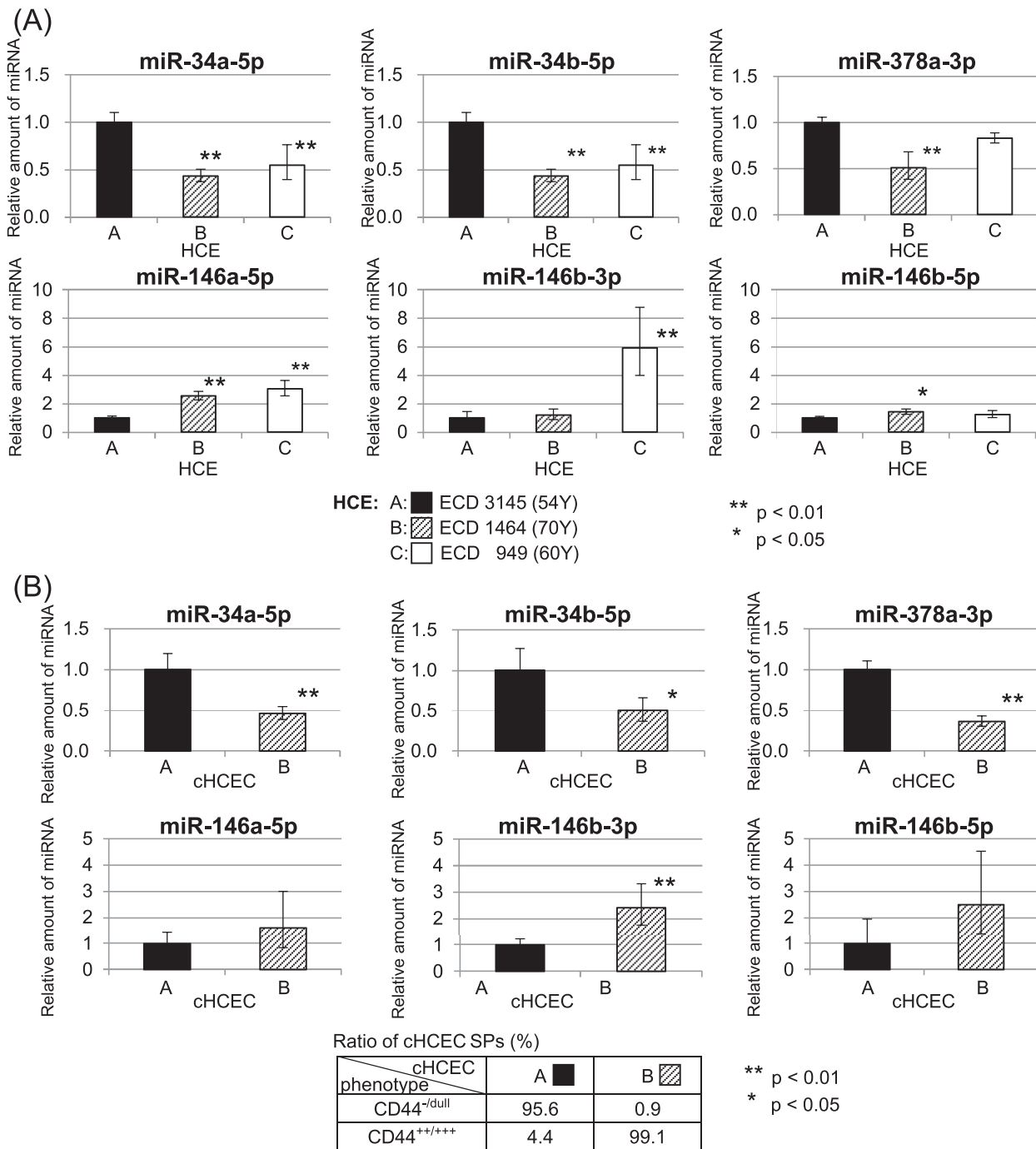


FIGURE 1. Repression of miR-34a/b and miR-378a in HCE tissues and cHCECs. **(A)** The expression levels of miR-34a/b-5p and miR-378-3p and three isoforms of control miR-146 (a-5p, b-3p, and b-5p) in HCE tissues with distinct ECDs (3145, 1463, and 949 cells/mm², respectively) were analyzed using a Toray 3D-Gene microarray. PCR was performed under the previously described conditions.^{10–12} The levels of miRs were normalized to that of GAPDH. The results are presented as relative units of expression. **(B)** The miR profiles were analyzed in two cHCEC SPs with distinct proportions of CD44^{-/-dull} cells (E-ratios = CD44^{-/-dull} cell proportions, 95.6% vs. 0.9%).

miRNA analysis. The volcano plots of miR profiles of fully matured SPs (CD44^{-/-dull}, 92.2%; CD44⁺, 7.8%) and intermediately matured SPs (CD44^{-/-dull}, 2.5%; CD44⁺, 84.3%) revealed the upregulation of miR-34a-5p in fully mature SPs, supporting the notion that miR-34a-5p expression is upregulated only at the stage of final maturation of cHCECs (Fig. 2C).

Cell Fate Decision by miR-34a/b in Immature cHCECs

The gene activation of IL-8, PDGF-ββ, and VEGF has been proven to be the biomarker in qualifying the differentiation status of cHCECs.^{10,11,16} The elevated IL-8 and VEGF, as well as the repressed PDGF-ββ gene expression, parallel the

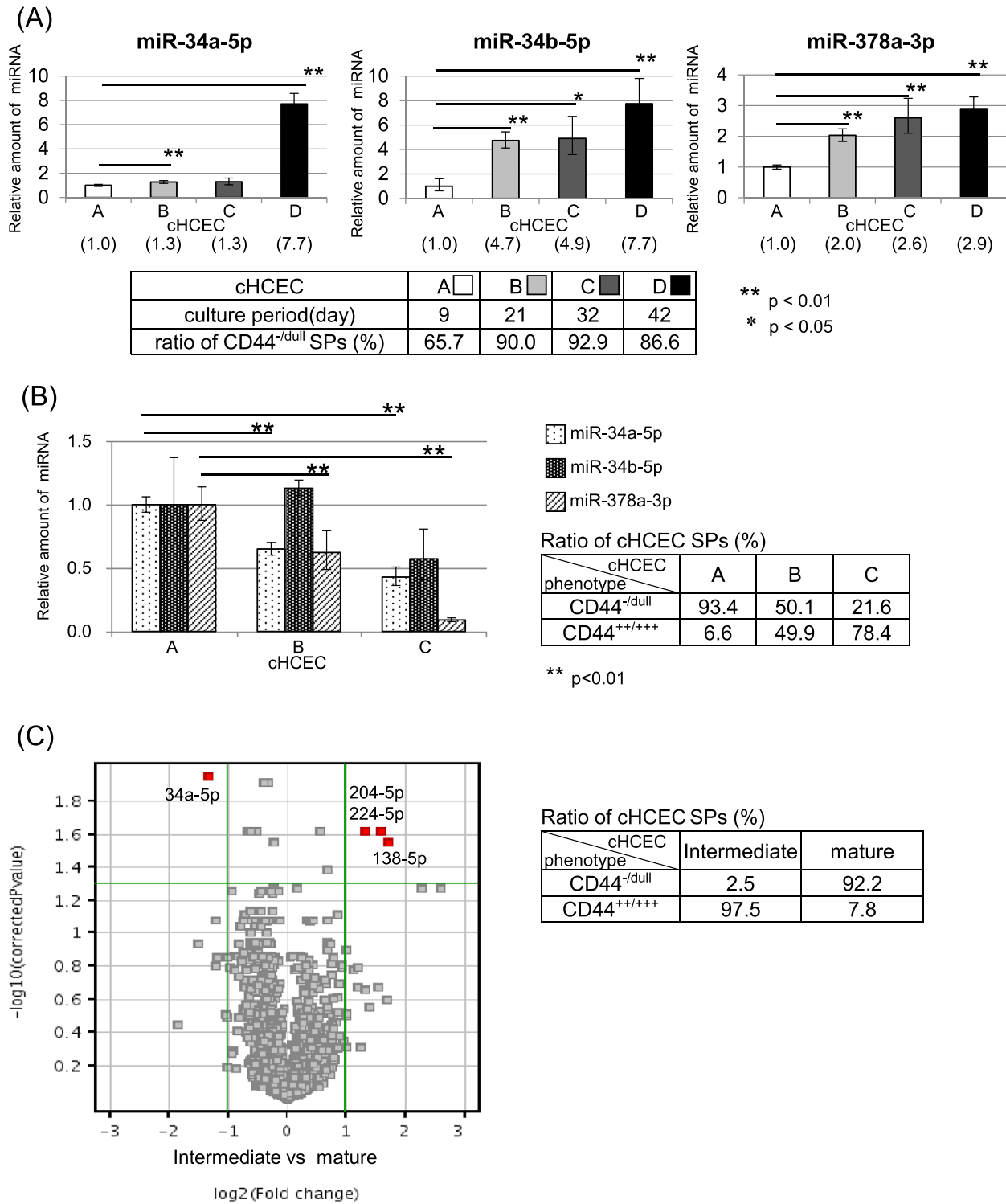


FIGURE 2. Repressed expression levels of miR-34a/b and miR-378a during culture period of cHCECs. **(A)** The periodic alteration of expression levels of miR-34a-5p, miR-34b-5p, and miR-378-3p during the culture stages was monitored. The expression levels of the latter two miRNAs were found to be already elevated at the differentiation stage on day 21, whereas that of miR-34a-5p was only elevated at the maturation stage on day 42. The analysis method was the same as that shown in Figure 1. **(B)** The altered expression levels of these miRNAs was reproducibly recognized among three cHCEC SPs with distinct CD44 expression levels (93.4%, 50%, and 21.6%). **(C)** A volcano plot of miR profiles of fully matured (CD44^{-/dull}, 92.2%; CD44^{+/+++}, 7.8%) and intermediately matured SPs (CD44^{-/dull}, 2.5%; CD44^{+/+++}, 84.3%).

elevated CD44 gene expression and the decreased proportion of cHCEC SPs with cell-surface CD44^{-/dull} (E-ratios). In the current study, the reproducibility of this principle to qualify the cellular features of cHCECs was confirmed among the cHCEC lots c33P3, C28 P5, and a3P3 with distinct E-ratios of 95.8%, 44.3%, and 0.9%, respectively (Fig. 3A). Aiming to clarify the direct participation in the cell-surface CD44 expression levels of miR-34a-5p and 34b-5p, the mimics for these miRs were transfected into day 6 cHCEC SPs with an E-ratio of 0.1% (lot a16) (Fig. 3B). RT-PCR conducted 48 hours after the transfection revealed the considerable repression of both of the miRs, although miR-34a-5p elicited more stable repression (Fig. 3B). The efficacy of the transfection was separately confirmed using small interfering RNA against GAPDH (siGAPDH), and the phenotype of responder day 6 cHCEC SPs with E-ratio 0.1% (lot a16) is illustrated in Supplementary Figure S1. The forced expression of the miR-34a-5p mimic also stably repressed IL-8 and VEGF and elevated PDGF- $\beta\beta$ gene expression in accordance with the repressed CD44 gene expression (Fig. 3C) (The responder cHCEC SP values for CD44, IL-8, and VEGF were 44.3% for CD44^{-/dull} and 53.3% for CD44^{+/+}; those for PDGF- $\beta\beta$ were 0.9% for CD44^{-/dull}, 22.5% for CD44^{+/+}, and 52.6% for CD44^{+/+/+}.) In contrast, the forced expression of miR-34b-5p inhibitor stably elevated IL-8 and VEGF and repressed the PDGF- $\beta\beta$ gene expression in accordance with the elevated CD44 gene expression (Fig. 3D). The inhibitor of miR-34a-5p significantly repressed PDGF- $\beta\beta$ inversely with the elevated CD44 gene expression, whereas no significant elevation was observed for IL-8 and VEGF gene expression levels. The responder cHCEC SP for CD44, IL-8, VEGF, and PDGF- $\beta\beta$ was 95.4% for CD44^{-/dull} (Fig. 3D).

miR34a-5p Mimics Lowers pHi and Restores Repressed Mitochondrial OXPHOS in CST cHCECs

Recently, we confirmed that pHi is lower in mature cHCEC SPs than in CST cHCEC SPs.^{10,11} The forced expression of miR-34a-5p mimic induces a statistically significant lowering of pHi (from none: 7.54 ± 0.19 to 7.10 ± 0.08 , $P = 0.00035$, $n = 12$; from control mimic: 7.13 ± 0.10 to 6.91 ± 0.11 , $P = 0.00045$, $n = 10$), consistent with the induction of cell phenotypes characteristic of the mature cHCECs described above (Fig. 4A).

In the Mito Stress Test, the forced expression of miR-34a-5p mimic into cHCECs (Supplementary Figs. S2A, S2B) showed a significant elevation ($*P < 0.05$) in the maximum OCR, but no significant downregulation of ECAR was observed (Fig. 4B), indicating the skewing to OXPHOS with no elevation of glycolysis by the transfection of miR-34a-5p mimic. We hypothesized the roles of miR-34a-5p and miR-34b-5p as illustrated in Figure 5. The differentiated mature HCECs might enter dedifferentiation, including EMT, to produce proliferative CD44^{+/+/+}, miR-34a-5p, and miR-34b-5p ^{-/dull} CST cHCEC SPs. Under the successive influence of both miR-34a-5p and miR-34b-5p, the CST cHCECs will differentiate and mature to differentiated mature cHCECs sharing almost similar phenotypes with the cells in fresh HCE tissues (Fig. 5).

p53 Participates in the Induction of miR-34a/b in Immature cHCECs

We next examined the induction of in immature cHCECs by p53. We selected the indirect assay of p53 activity in cHCECs

by measuring the induction of p21 protein by an MDM2 inhibitor, Nutlin-3a, because Nutlin-3a is expected to stabilize and activate p53 protein.^{36,37} The accumulation of p53 and p21 in parallel was verified with a WB analysis (Fig. 6). Meanwhile, there was a clear upregulation of miR-34a and miR-34b with the increased concentration of Nutlin-3a that was added (2–5 mM). These results indicate that Nutlin-3a causes the accumulation of and increase in the transcriptional activity of p53 to upregulate the lowered levels of miR-34a and miR-34b in immature cHCEC SPs.

Correlation of MiR34a and Proteins Responsible for the Cellular Cytoskeleton, Rho A, and MMP-2

The miR-34a/c-Myc axis regulated the CD44 expression and its downstream factors: Rho A and MMP-2.³⁸ Cultured HCECs with increased levels of cell-surface CD44 expression elicited a positive correlation with increased Rho A activity, as evidenced by a lower level of guanosine-5'-triphosphate (GTP)-bound Rho A (Fig. 7A). The immunoblotting showed that the level of intracellular MMP-2 protein was also positively correlated with the expression level of CD44 and inversely correlated with that of miR-34a-5p in cHCECs (Fig. 7B). These results were supported by those obtained by immunocytological staining, which showed the increased level of MMP-2 selectively in CD44^{+/+/+} immature cHCECs but not in CD44^{-/dull} mature cHCECs (Fig. 7C).

Exposure to H₂O₂ Represses miR-34a Expression

Equal amounts of protein derived from mature differentiated cHCEC SPs exposed to 1-mM H₂O₂ for 4 or 24 hours were applied in WB. The gene product c-Myc, which is reportedly regulated by miR-34a, was remarkably upregulated, although the activation of p53, known as an miR-34a regulator, was moderate or absent. The mitochondria biogenesis-related proteins SIRT1 and DJ-1 did not elicit distinct responses, whereas PGC1- α , which is most responsible for mitochondrial biogenesis, was downregulated. The mitochondrial markers TOMM20 and TFAM showed decreased expression. As expected, oxidative stress-induced DNA damage-related cellular proteins, phospho-H2AX, Nrf2, and HO-1, were all upregulated (Fig. 8A).

c-Myc can make the cells addicted to specific bioenergetic substrates.³⁹ In this context, c-Myc also regulates the expression of CD44, which is a key molecule in distinguishing between differentiated cHCECs and cHCECs with CST (our published observations).⁴⁰ Differentiated cHCECs exposed to H₂O₂ for 24 hours clearly upregulated the expression levels of both c-Myc (Fig. 8A) and CD44 (Fig. 8A), indicating that the oxidative stresses exposed on differentiated mature HCECs are the causal cellular stress, albeit in part, that induces their degeneration with the impaired mitochondrial homeostasis (lowered TOMM20 and TFAM) in HCECs. The expression levels of miR-34a ($P = 0.034$)/miR-34b ($P = 0.021$), and miR-378a ($P = 0.012$) after 24 hours of exposure to 1-mM H₂O₂ were clearly repressed in parallel with the upregulated expression of CD44 ($P = 0.006$) (Fig. 8B).

DISCUSSION

A recent landmark study conducted by our group has demonstrated that the intracameral injection of cHCECs can reverse corneal edema with stable clinical outcomes in patients with bullous keratopathy and Fuchs' endothelial

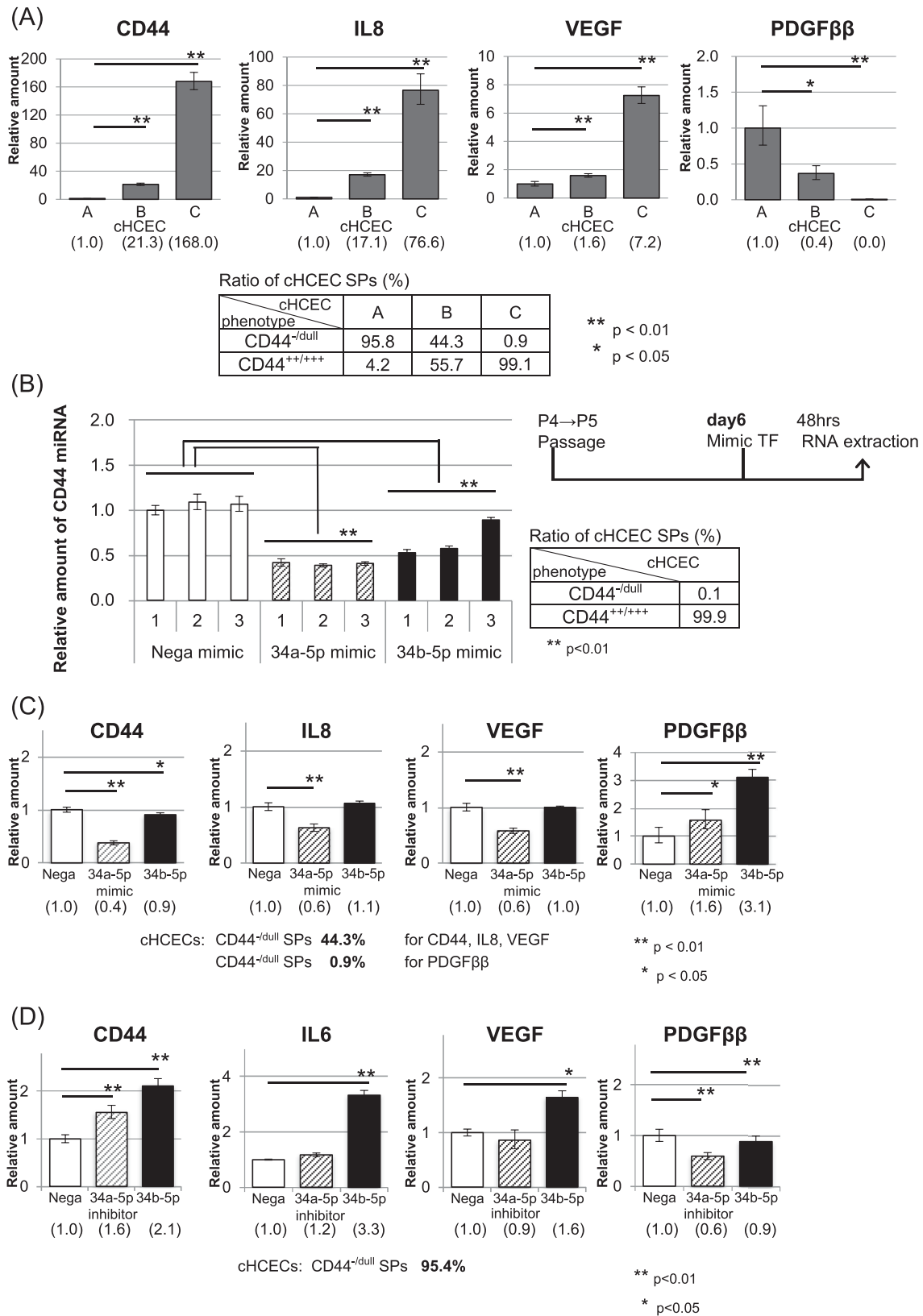


FIGURE 3. Cell fate decision by miR-34a/b in immature cHCECs. **(A)** Gene activation of IL-8, PDGF-β, and VEGF, which are useful biomarkers for qualifying the differentiation status of cHCECs, as well as that of CD44 among the three cHCECs with distinct proportions of CD44^{-/dull} SPs (A, B, C: 95.8%, 44.3%, and 0.9%, respectively), was analyzed by RT-PCR. **(B)** The cell-surface CD44 expression on cHCECs was directly regulated by the transfection of miR-34a-5p and miR-34b-5p mimics. These miRs were transfected into day 6 cHCEC SPs with an E-ratio of 0.1%. RT-PCR was performed 48 hours after the transfection. **(C)** The forced expression of miR-34a-5p mimic also stably repressed IL-8 and

VEGF and elevated PDGF-β gene expression in accordance with the repressed CD44 gene expression. (The responder cHCEC SP values for CD44, IL-8, and VEGF were 44.3% for CD44^{-/dull} and 53.3% for CD44^{+/+}; those for PDGF-β were 0.9% for CD44^{-/dull}, 22.5% for CD44^{+/+}, and 52.6% for CD44^{+/+/+}.) (D) The forced expression of miR-34b-5p inhibitor stably elevated IL-8 and VEGF and repressed PDGF-β gene expression in accordance with the elevated CD44 gene expression. The inhibitor of miR-34a-5p significantly repressed PDGF-β inversely with the elevated CD44 gene expression. The responder cHCEC SP for CD44, IL-8, VEGF, and PDGF-β was CD44^{-/dull} 95.4%.

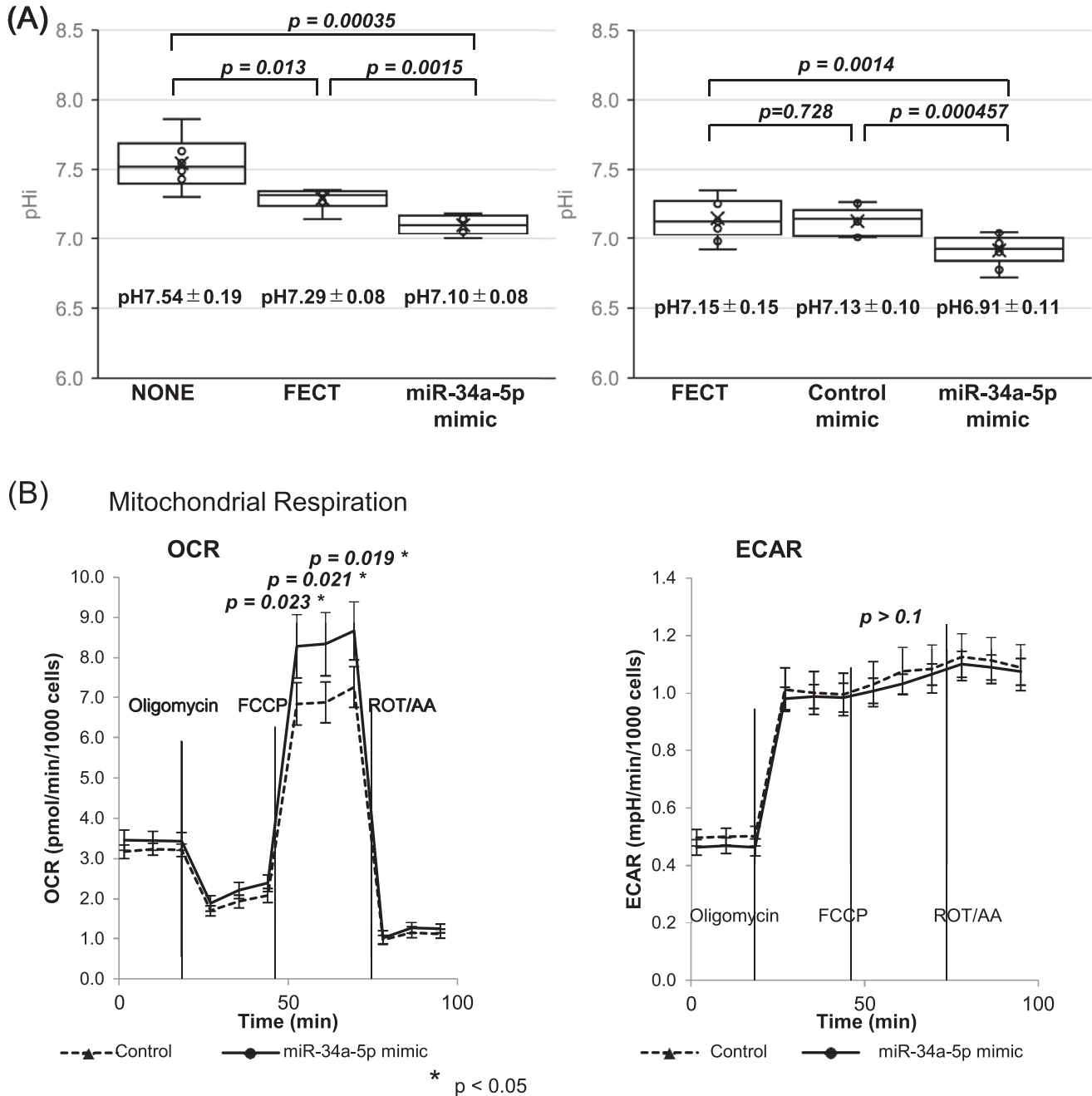


FIGURE 4. miR34a-5p mimics lower pHi and restore represses mitochondrial OXPHOS in CST cHCECs. (A) The forced expression of miR-34a-5p mimic lowered pHi (from 7.54 ± 0.191 to 7.10 ± 0.075; P = 0.00035; n = 12). (B) In the Mito Stress Test, the forced expression of miR-34a-5p mimic showed a significant elevation (*P < 0.05) in the maximum OCR, but no significant downregulation of ECAR was observed.

corneal dystrophy (FECD).^{8,9,13} We have successfully distinguished between cHCEC SPs with high clinical efficacy (the SPs are described as effector cells) and those with low effi-

cacy. The former elicited cellular phenotypes almost the same as those of fresh tissue HCEs, whereas the latter elicited a clear distinction from them.¹⁰⁻¹⁶ In addition, mitochondrial

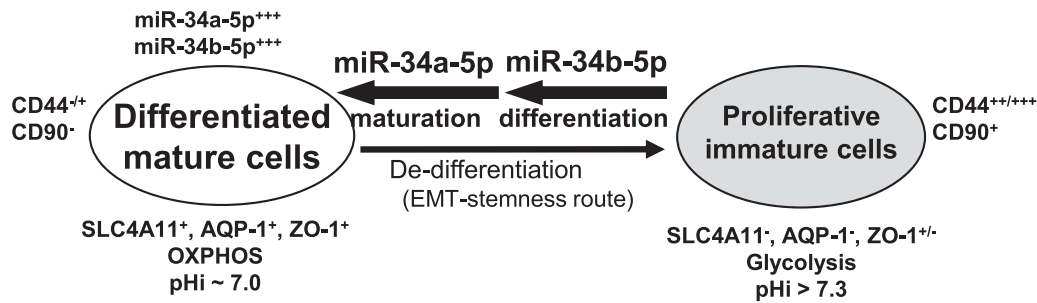


FIGURE 5. Hypothesis for the induction of mature differentiated HCE cells. The differentiated mature HCECs in HCE tissues might enter dedifferentiation to produce proliferative CD44^{+/+/+}, miR-34a-5p, and miR-34b-5p -/dull cHCEC SPs. Under the successive influence of both miR-34a-5p and miR-34b-5p, the CST cHCECs will differentiate and mature to mature differentiated cHCECs sharing almost similar phenotypes (neutral pHi, SLC4A11⁺, AQP⁺, and disposed to mitochondrial OXPPOS) with the cells in fresh HCE tissues.

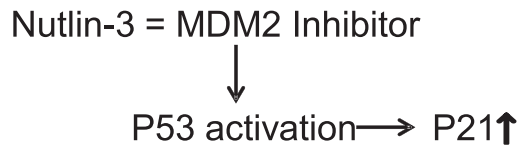
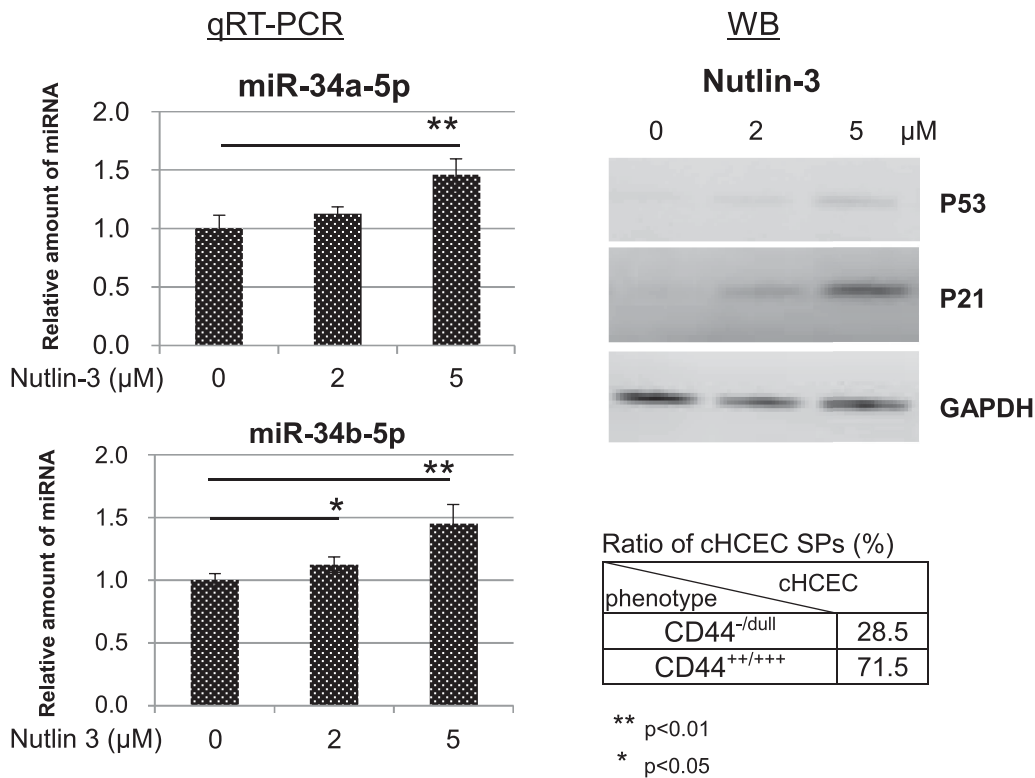


FIGURE 6. p53 participates in miR-34a/b induction in immature cHCECs. The indirect assay of p53 activity in cHCECs obtained by measuring the induction of p21 protein by an MDM2 inhibitor, Nutlin-3a, was selected. The accumulation of p53 and p21 in parallel was verified with a WB analysis, and Nutlin-3a was found to upregulate the expression levels of miR-34a and miR-34b (qRT-PCR). The responder cHCECs used were CD44^{-/-dull} 28.5%. The experiments were repeated three times, and the representative results are presented.

OXPPOS in the effector SPs was more dominant, whereas glycolysis and OXPPOS were both elevated in cHCEC SPs with CST, including dedifferentiation, EMT, immaturity, and cell senescence.^{10,11}

In fresh HCE tissues, we observed contrasting miR signatures. The miRs related to EMT were upregulated in HCE tissues with low ECD.⁴⁰ The miR-34a and miR-378 family was downregulated in HCE tissues with low ECD and in cHCECs

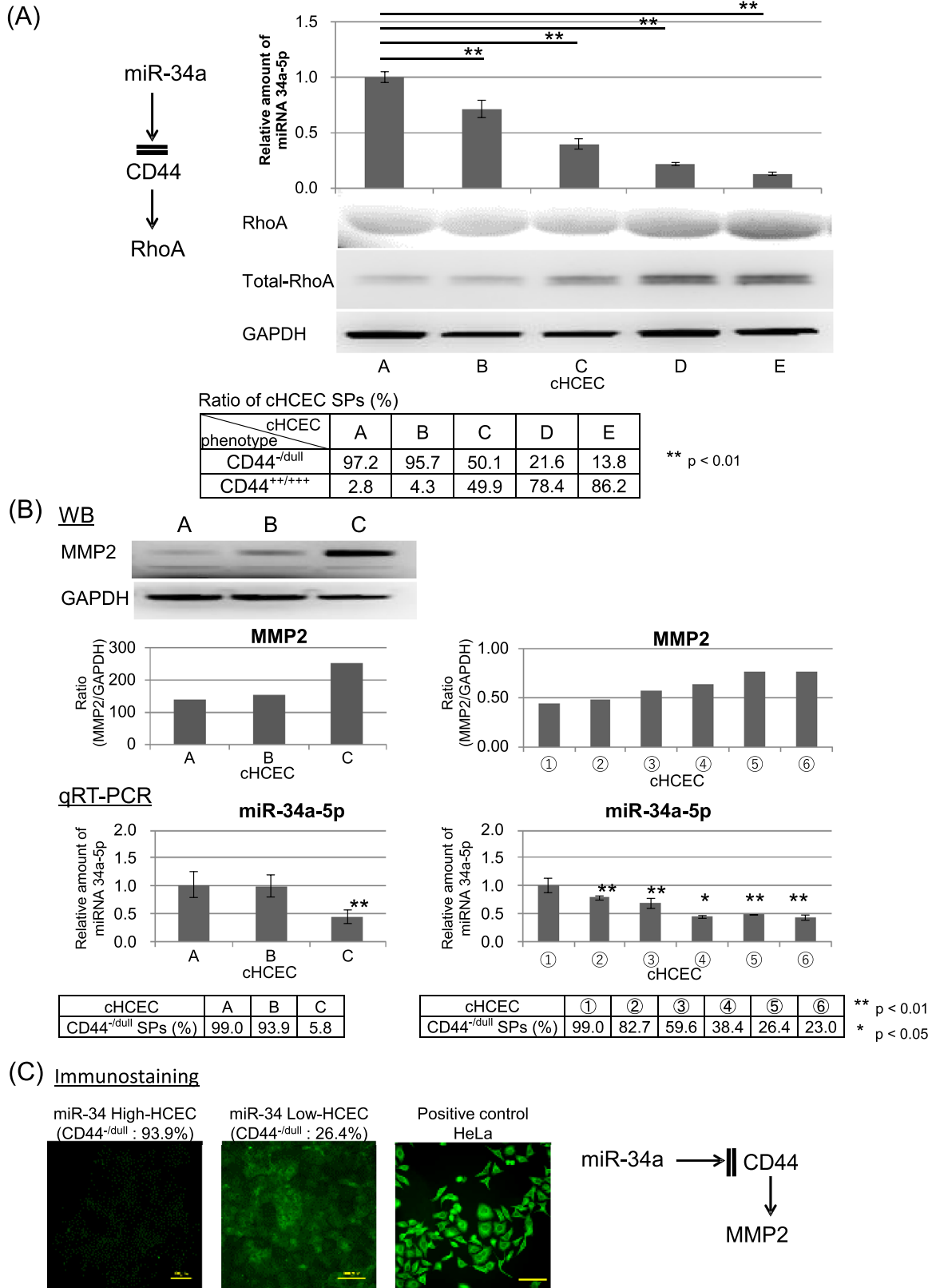


FIGURE 7. Correlation of miR-34a and CD44 downstream proteins responsible for the cellular cytoskeleton, Rho A and MMP-2. **(A)** Five cHCECs with increased levels of cell-surface CD44 expression elicited a positive correlation with increased Rho A activity, as evidenced by a lower level of GTP-bound Rho A. Reagents from the Cytoskeleton RhoA Pull-Down Activation Assay Biochem Kit were added to the protein lysates according to the manufacturer's instructions. WB was then performed on the proteins that remained bound to the beads by using a special Rho A primary antibody provided by the manufacturer. **(B)** The immunoblotting showed that the level of intracellular MMP-2 protein

was positively correlated with the expression levels of CD44 among three and six independent cHCEC SPs (A, B, C and 1–6) and inversely correlated with miR-34a-5p expression in these cHCECs (qRT-PCR). The experiment was repeated in duplicate, and the average expression intensity over GAPDH is depicted. (C) The immunocytochemical staining increased the level of MMP-2 selectively in CD44^{+/+/+} immature cHCECs but not in CD44^{-/duall} mature cHCECs. HeLa cells were stained under the same condition as those used for a positive control.

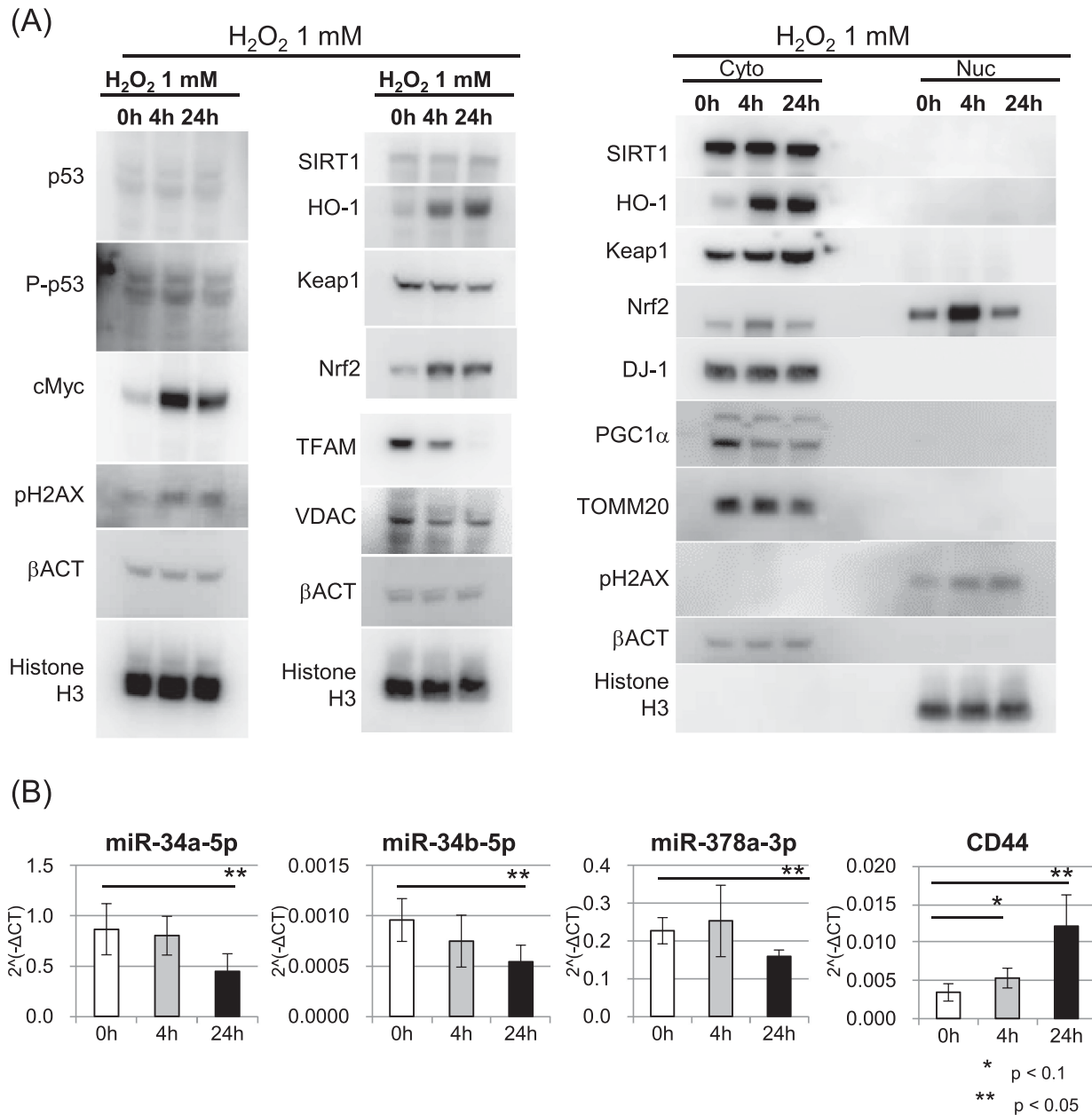
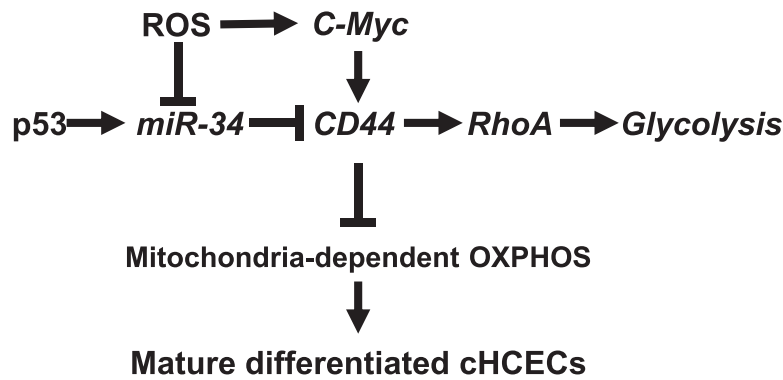


FIGURE 8. Exposure to H₂O₂ regulates the mitochondrial homeostasis and inversely represses miR-34a expression with the elevation of CD44 expression. (A) Equal amounts of protein derived from mature differentiated cHCEC SPs exposed to 1-mM H₂O₂ for 4 or 24 hours were applied in WB. c-Myc was upregulated, and the activation of p53 was moderate or absent, whereas PGC1-α was downregulated. Mitochondrial markers TOMM20, VDAC, and TFAM showed decreased expression levels. DNA-damage-related cellular proteins (phospho-H2AX, Nrf2, and HO-1) were all upregulated. (B) Differentiated mature cHCECs exposed to H₂O₂ for 24 hours clearly upregulated CD44 expression. The expression levels of miR-34a (*P* = 0.034)/miR-34b (*P* = 0.021) and miR-378a (*P* = 0.012) after exposure to 1-mM H₂O₂ for 24 hours were clearly repressed in parallel with the upregulated expression of CD44 (*P* = 0.006). All data were globally normalized according to the manufacturer's protocol. All experiments for (A) and (B) were repeated four times, and representative data are shown.

with low proportions of effector cells (Fig. 1). In the current study, we confirmed the inverse association of the expression levels of miR-34a/b and miR-378a during the distinct

culture stages of HCECs (proliferation, differentiation, and maturation), with the progressively repressed gene expression of cell-surface CD44 (Fig. 2A), in addition to directly



ROS: reactive oxygen species

FIGURE 9. Schematic hypothesis regarding the cell fate disposition to OXPHOS skewed HCEC. Differentiated mature HCECs dominant in OXPHOS exhibited a disposition for anaerobic glycolysis instead of mitochondria-dependent OXPHOS under the ROS-induced upregulation of CD44 through the downregulation of miR-34a and upregulation of c-Myc.

confirming that miR-34a downregulates CD44 expression (Figs. 3B–3D) and that the miR-34a/CD44 axis activates the downstream factors of CD44, including Rho A and MMP-2 (Fig. 7), which are responsible for the organization of tubulin and actin cytoskeleton.³⁸ The findings here have raised the novel notion that the oxidative cellular stress causing degenerated cHCECs is accompanied by reduced miR-34a expression (Fig. 8B) and a reduction in mitochondria biogenesis (refer to TFAM, VDAC, and TOMM20 gene expression levels) through the reduced PGC-1 α signaling cascade (Fig. 8A). PGC-1 α regulates mitochondrial biogenesis and oxidative metabolism by activating many transcription factors, including Nrf2.^{41,42} Oxidative stress plays a major role in the chronic degenerative process of the corneal endothelium and CEC apoptosis observed in FECD.^{43–46} Under oxidative stress, reactive oxygen species (ROS) induce modifications in the Nrf2–Keap1 complex, which lead to Nrf2 dissociation from Keap1 and enable Nrf2 translocation to the nucleus to activate the antioxidant responsive element (ARE).

The above-mentioned observation supports our newly proposed hypothesis on the cell fate decision process, as shown in Figure 9. Differentiated mature CD44^{-dull} cHCEC SPs dominant in OXPHOS exhibit a disposition for anaerobic glycolysis instead of mitochondria-dependent OXPHOS under oxidative stress through the downregulation of miR-34a. The mitochondrial respiratory function is dynamically plastic in response to the upregulation of CD44 expression through c-Myc, upregulated directly by ROS or indirectly by repressed miR-34a induced by decreased p53 activity, which is also regulated by ROS. Interestingly, p53 suppresses the Nrf2-dependent transcription of ARE-dependent genes, and there is a negative correlation between Nrf2 and p53 activity.⁴⁷ In this study, we confirmed that the Nutlin-3-induced activation of p53→p21 was well correlated with the upregulated expression levels of miR-34a-5p and miR-34b-5p (Fig. 6), indicating the upstream role of p53 in ROS-induced downregulation of these miRs. A positive correlation exists between miR-34a and p53 in a SIRT1–p53-dependent pathway, and miR-34a can regulate both SIRT1 and Nrf2.⁴⁸

There are several reports that pHi is directly related to the mitochondrial function and indirectly to cell differentiation in other cells.^{24–32} In this context, we hypothesized that pHi regulated directly or indirectly by miR-34a in HCECs is associated with mitochondrial homeostasis (Fig. 4). pHi can regu-

late not only the cell fate, such as differentiation versus CST, dedifferentiation, or EMT, but also mitochondrial homeostasis and is consequently associated with the efficient water efflux from corneal stroma to the AC of cHCEC effector SPs.

In 2007, several researchers determined that members of the miR-34 family are the most prevalent p53-induced miRNAs.⁴⁹ The present study has demonstrated for the first time, to the best of our knowledge, that the miR-34a/CD44 pathway regulates the mitochondria-dependent bioenergetics impaired by ROS-induced cellular stress. The c-Myc/miR-34a axis regulates the cellular cytoskeleton by mediating the expression and/or activation of CD44, including Rho A and MMP-2,³⁸ as well as the disposition to mitochondrial OXPHOS. CD44 ablation increases metabolic flux to mitochondrial respiration and concomitantly inhibits entry into glycolysis.⁵⁰

To clarify the distinction between in vitro CST cHCECs and degenerated HCE tissues, it is quite critical to extend this study further from the standpoint of morphology and morphometry.

Acknowledgments

The authors thank Asako Uehara and Michio Hagiya for their technical assistance and Keiko Takada and Yoko Hamuro for their secretarial assistance throughout the study.

Supported by the Projects for Technological Development from Japan Agency for Medical Research and Development (MED 19bm0404033h0002) and by a grant from Japan Society for the Promotion of Science KAKENHI (JP26293376).

Disclosure: **J. Hamuro**, None; **K. Asada**, None; **M. Ueno**, None; **T. Yamashita**, None; **A. Mukai**, None; **T. Fujita**, None; **E. Ito**, None; **N. Hiramoto**, None; **M. Toda**, None; **C. Sotozono**, None; **S. Kinoshita**, None

References

1. Tuft SJ, Coster DJ. The corneal endothelium. *Eye*. 1990;4(Pt 3):389–424.
2. Wörner CH, Olguín A, Ruíz-García JL, Garzón-Jiménez N. Cell pattern in adult human corneal endothelium. *PLoS One*. 2011;6(5):e19483.

3. Bonanno JA. Molecular mechanisms underlying the corneal endothelial pump. *Exp Eye Res.* 2012;95(1):2–7.
4. Sie NM, Yam GH, Soh YQ, et al. Regenerative capacity of the corneal transition zone for endothelial cell therapy. *Stem Cell Res Ther.* 2020;11(1):523.
5. Writing Committee for the Cornea Donor Study Research Group, Lass JH, Benetz BA, et al. Donor age and factors related to endothelial cell loss 10 years after penetrating keratoplasty: specular microscopy ancillary study. *Ophthalmology.* 2013;120(12):2428–2435.
6. Price MO, Calhoun P, Kollman C, Price FW, Jr, Lass JH. Descemet stripping endothelial keratoplasty: ten-year endothelial cell loss compared with penetrating keratoplasty. *Ophthalmology.* 2016;123(7):1421–1427.
7. Melles GR, Ong TS, Ververs B, van der Wees J. Preliminary clinical results of Descemet membrane endothelial keratoplasty. *Am J Ophthalmol.* 2008;145(2):222–227.
8. Kinoshita S, Koizumi N, Ueno M, et al. Injection of cultured cells with a ROCK inhibitor for bullous keratopathy. *N Engl J Med.* 2018;378(11):995–1003.
9. Numa K, Imai K, Ueno M, et al. Five-year follow-up of first 11 patients undergoing injection of cultured corneal endothelial cells for corneal endothelial failure. *Ophthalmology.* 2021;128(4):504–514.
10. Hamuro J, Numa K, Fujita T, et al. Metabolites interrogation in cell fate decision of cultured human corneal endothelial cells. *Invest Ophthalmol Vis Sci.* 2020;61(2):10.
11. Numa K, Ueno M, Fujita T, et al. Mitochondria as a platform for dictating the cell fate of cultured human corneal endothelial cells. *Invest Ophthalmol Vis Sci.* 2020;61(14):10.
12. Toda M, Ueno M, Hiraga A, et al. Production of homogeneous cultured human corneal endothelial cells indispensable for innovative cell therapy. *Invest Ophthalmol Vis Sci.* 2017;58(4):2011–2020.
13. Ueno M, Toda M, Numa K, et al. Superiority of mature differentiated cultured human corneal endothelial cell injection therapy for corneal endothelial failure. *Am J Ophthalmol.* 2021;237:267–277.
14. Hamuro J, Toda M, Asada K, et al. Cell homogeneity indispensable for regenerative medicine by cultured human corneal endothelial cells. *Invest Ophthalmol Vis Sci.* 2016;57(11):4749–4761.
15. Hamuro J, Ueno M, Toda M, Sotozono C, Montoya M, Kinoshita S. Cultured human corneal endothelial cell aneuploidy dependence on the presence of heterogeneous subpopulations with distinct differentiation phenotypes. *Invest Ophthalmol Vis Sci.* 2016;57(10):4385–4392.
16. Hamuro J, Ueno M, Asada K, et al. Metabolic plasticity in cell state homeostasis and differentiation of cultured human corneal endothelial cells. *Invest Ophthalmol Vis Sci.* 2016;57(10):4452–4463.
17. Deguchi H, Yamashita T, Hiramoto N, et al. Intracellular pH affects mitochondrial homeostasis in cultured human corneal endothelial cells prepared for cell injection therapy. *Sci Rep.* 2022;12(1):6263.
18. Vilas GL, Loganathan SK, Liu J, et al. Transmembrane water flux through SLC4A11: a route defective in genetic corneal diseases. *Hum Mol Genet.* 2013;22(22):4579–4590.
19. Eghrari AO, Riazuddin SA, Gottsch JD. Fuchs corneal dystrophy. *Prog Mol Biol Transl Sci.* 2015;134:79–97.
20. Alka K, Casey JR. Molecular phenotype of SLC4A11 missense mutants: setting the stage for personalized medicine in corneal dystrophies. *Hum Mutat.* 2018;39(5):676–690.
21. Meng H, Matthaai M, Ramanan N, et al. L450W and Q455K Col8a2 knock-in mouse models of Fuchs endothelial corneal dystrophy show distinct phenotypes and evidence for altered autophagy. *Invest Ophthalmol Vis Sci.* 2013;54(3):1887–1897.
22. Riazuddin SA, Eghrari AO, Al-Saif A, et al. Linkage of a mild late-onset phenotype of Fuchs corneal dystrophy to a novel locus at 5q33.1-q35.2. *Invest Ophthalmol Vis Sci.* 2009;50(12):5667–5671.
23. Patel SP, Parker MD. SLC4A11 and the pathophysiology of congenital hereditary endothelial dystrophy. *Biomed Res Int.* 2015;2015:475392.
24. Masereel B, Pochet L, Laeckmann D. An overview of inhibitors of Na⁺/H⁺ exchanger. *Eur J Med Chem.* 2003;38(6):547–554.
25. Li X, Karki P, Lei L, Wang H, Fliegel L. Na⁺/H⁺ exchanger isoform 1 facilitates cardiomyocyte embryonic stem cell differentiation. *Am J Physiol Heart Circ Physiol.* 2009;296(1):H159–H170.
26. Javadov S, Rajapurohitam V, Kilić A, Zeidan A, Choi A, Karmazyn M. Anti-hypertrophic effect of NHE-1 inhibition involves GSK-3 β -dependent attenuation of mitochondrial dysfunction. *J Mol Cell Cardiol.* 2009;46(6):998–1007.
27. Gao W, Zhang H, Chang G, et al. Decreased intracellular pH induced by cariporide differentially contributes to human umbilical cord-derived mesenchymal stem cells differentiation. *Cell Physiol Biochem.* 2014;33(1):185–194.
28. Ulmschneider B, Grillo-Hill BK, Benitez M, Azimova DR, Barber DL, Nystul TG. Increased intracellular pH is necessary for adult epithelial and embryonic stem cell differentiation: pH regulates stem cell differentiation. *J Cell Biology.* 2016;215(3):345–355.
29. Fang Y, Liu Z, Chen Z, et al. Smad5 acts as an intracellular pH messenger and maintains bioenergetic homeostasis. *Cell Res.* 2017;27(9):1083–1099.
30. Sanhueza C, Araos J, Naranjo L, et al. Sodium/proton exchanger isoform 1 regulates intracellular pH and cell proliferation in human ovarian cancer. *Biochim Biophys Acta Mol Basis Dis.* 2017;1863(1):81–91.
31. Hyun SY, Na EJ, Jang JE, et al. Induction of apoptosis and differentiation by Na/H exchanger 1 modulation in acute myeloid leukemia cells. *Biochem Biophys Res Commun.* 2019;519(4):887–893.
32. Genders AJ, Martin SD, McGee SL, Bishop DJ. A physiological drop in pH decreases mitochondrial respiration, and HDAC and Akt signaling, in L6 myocytes. *Am J Physiol Cell Physiol.* 2019;316(3):C404–C414.
33. Ueno M, Asada K, Toda M, et al. Concomitant evaluation of a panel of exosome proteins and MiRs for qualification of cultured human cornea endothelial cells. *Invest Ophthalmol Vis Sci.* 2016;57(10):4393–4402.
34. Nomura K, Klejnot M, Kowalczyk D, et al. Structural analysis of MDM2 RING separates degradation from regulation of p53 transcription activity. *Nat Struct Mol Biol.* 2017;24(7):578–587.
35. Meijer A, Kruyt FA, van der Zee AG, et al. Nutlin-3 preferentially sensitises wild-type p53-expressing cancer cells to DR5-selective TRAIL over rhTRAIL. *Br J Cancer.* 2013;109(10):2685–2695.
36. Chang LJ, Eastman A. Differential regulation of p21 (waf1) protein half-life by DNA damage and Nutlin-3 in p53 wild-type tumors and its therapeutic implications. *Cancer Biol Ther.* 2012;13(11):1047–1057.
37. Deben C, Wouters A, Op de Beeck K, et al. The MDM2-inhibitor Nutlin-3 synergizes with cisplatin to induce p53 dependent tumor cell apoptosis in non-small cell lung cancer. *Oncotarget.* 2015;6(26):22666–22679.
38. Lin L, Jiang H, Huang M, et al. Depletion of histone deacetylase 1 inhibits metastatic abilities of gastric cancer cells by regulating the miR-34a/CD44 pathway. *Oncol Rep.* 2015;34(2):663–672.
39. Davidson SM, Vander Heiden MG. METabolic adaptations in the tumor MYCenvironment. *Cell Metab.* 2012;15(2):131133.

40. Ueno M, Asada K, Toda M, et al. MicroRNA profiles qualify phenotypic features of cultured human corneal endothelial cells. *Invest Ophthalmol Vis Sci.* 2016;57(13):5509–5517.
41. Jung S, Kim K. Exercise-induced PGC-1 α transcriptional factors in skeletal muscle. *Integr Med Res.* 2014;3(4):155–160.
42. Yang S, Hwang S, Jang J, Kim M, Gwak J, Jeong SM. PGC1 α is required for the induction of contact inhibition by suppressing ROS. *Biochem Biophys Res Commun.* 2018;501(3):739–744.
43. Bitar MS, Liu C, Ziaei A, Chen Y, Schmedt T, Jurkunas UV. Decline in DJ-1 and decreased nuclear translocation of Nrf2 in Fuchs endothelial corneal dystrophy. *Invest Ophthalmol Vis Sci.* 2012;53(9):5806–5813.
44. Jurkunas UV, Bitar MS, Funaki T, Azizi B. Evidence of oxidative stress in the pathogenesis of Fuchs endothelial corneal dystrophy. *Am J Pathol.* 2010;177(5):2278–2289.
45. Azizi B, Ziaei A, Fuchsluger T, Schmedt T, Chen Y, Jurkunas UV. p53-regulated increase in oxidative-stress-induced apoptosis in Fuchs endothelial corneal dystrophy: a native tissue model. *Invest Ophthalmol Vis Sci.* 2011;52(13):9291–9297.
46. Wang Z, Handa JT, Green WR, Stark WJ, Weinberg RS, Jun AS. Advanced glycation end products and receptors in Fuchs' dystrophy corneas undergoing Descemet's stripping with endothelial keratoplasty. *Ophthalmology.* 2007;114(8):1453–1460.
47. Faraonio R, Vergara P, Di Marzo D, et al. p53 suppresses the Nrf2-dependent transcription of antioxidant response genes. *J Biol Chem.* 2006;281(52):39776–39784.
48. Akbari G, Mard SA, Dianat M, Mansouri E. The hepatoprotective and microRNAs downregulatory effects of crocin following hepatic ischemia-reperfusion injury in rats. *Oxid Med Cell Longev.* 2017;2017:1702967.
49. He L, He X, Lowe SW, Hannon GJ. MicroRNAs join the p53 network—another piece in the tumour-suppression puzzle. *Nat Rev Cancer.* 2007;7(11):819–822.
50. Tamada M, Nagano O, Tateyama S, et al. Modulation of glucose metabolism by CD44 contributes to antioxidant status and drug resistance in cancer cells. *Cancer Res.* 2012;72(6):1438–1448.